Theoretical study of the electronic spectroscopy of CO adsorbed on Pt(111)

Nicholas A. Besley[a)]
School of Chemistry, University of Nottingham, University Park, Nottingham NG7 2RD, United Kingdom

(Received 15 December 2004; accepted 23 February 2005; published online 10 May 2005)

The excited states of CO adsorbed on the Pt(111) surface are studied using a time-dependent density functional theory formalism. To reduce the computational cost, electronic excitations are computed within a reduced single excitation space. Using cluster models of the surface, excitation energies are computed for CO in the on-top, threefold, and bridge binding sites. On adsorption, there is a lowering of the 5σ orbital energy. This leads to a large blueshift in the $5\sigma \rightarrow \pi^*_{CO}$ excitation energy for all adsorption sites. The 1π and 4σ orbital energies are lowered to a lesser extent, and smaller shifts in the corresponding excitation energies are predicted. For the larger clusters, π^* excitations at lower energies are observed. These transitions correspond to excitations to virtual orbitals of π^* character which lie below the π^* orbitals of gas phase CO. These orbitals are associated predominantly with the metal atoms of the cluster. The excitation energies are also found to be sensitive to changes in the adsorption geometry. The electronic spectrum of CO on Pt(111) is simulated and the assignment of the bands observed in experimental electron energy loss spectroscopy discussed. © *2005 American Institute of Physics*. [DOI: 10.1063/1.1891687]

I. INTRODUCTION

Advances in methodologies and computational resources have made it possible to study a diverse range of problems using quantum chemistry. Surface science is an area of research that has exploited quantum chemistry extensively. The aim of much of this research is to establish the location and structure of adsorbed molecules and determine the strength of their interaction with the surface. In particular, density functional theory (DFT) has been used with supercell or cluster models of the surface to study a variety of systems. Such theoretical work can elucidate experimental findings and provide a detailed picture of the adsorption process at a molecular orbital level, in an effort to understand why a molecule adsorbs in a particular way.[1] The vast majority of work in surface science considers the adsorbed molecule and surface to be in their electronic ground state. However, the study of the electronically excited states of adsorbed molecules is important in fields such as photochemistry and photoluminescence at surfaces.[2–4] Furthermore, the study of excited states yields information about the changes in electronic structure that occur on adsorption, and this can provide additional insight into the adsorption process.

The adsorption of carbon monoxide on transition metal surfaces is often used as a prototypical system in surface science and has been discussed extensively in the literature, for example, Refs. 1 and 5–12. In gas phase, the highest occupied molecular orbital (HOMO) of CO is the 5σ orbital. This orbital is located mainly on the carbon atom. Below the 5σ orbital lie the two bonding 1π orbitals, while the lowest unoccupied molecular orbitals (LUMOs) are the two antibonding $2\pi^*$ orbitals. The interaction between carbon monoxide and a transition metal surface is usually described in terms of these orbitals and the *d* band of the metal. This leads to the idea of forward donation from the 5σ orbital of CO to the metal and back donation from the metal to the antibonding $2\pi^*$ orbitals of CO, in the so-called Blyholder model.[5] Although in the original work of Blyholder only the π electronic structure was discussed. In an effort to understand the adsorption behavior of CO, Hoffmann and co-workers[1,7,13] reported a detailed analysis of the interactions between the orbitals of CO and metal surfaces. The HOMO of CO lies below the *d* band of transition metals. The 5σ orbital interacts with the *d* band and the empty *s* and *p* surface bands and is pushed down in energy.[13] This interaction has been found to be strongest for the on-top binding site, and decreases in the twofold (bridge) and threefold (fcc hollow) sites.[1] These predictions were based on extended Hückel theory, which can be unreliable. The π orbitals also interact with the metal *d* band. For the on-top and threefold binding sites the degeneracy of the π orbitals is retained, while for the twofold site this degeneracy is lifted.[1] In general, the Blyholder model was found to be valid with its major deficiency being the neglect of the 4σ orbital. Subsequently, other authors have also addressed the validity of the Blyholder model.[8,9,11,14–16] In plane wave supercell calculations of the adsorption of CO on Pd(110), Hu *et al.* found significant mixing of the $4\sigma, 5\sigma, 1\pi$, and $2\pi^*$ orbitals with the orbitals of the metal atoms.[8] This introduced metal-5σ and metal-$2\pi^*$ bonding and antibonding states. It was concluded that the Blyholder model was oversimplistic and that the band structure of the system should be considered. The Blyholder model has also been criticized due to the $2\pi^*$ state lying above the Fermi energy.[14,15] However, alternative studies have been supportive of the Blyholder model.[9,11] Overall, while there is significant mixing of the CO and metal orbitals, the idea of forward

[a)]Electronic mail: nick.besley@nottingham.ac.uk

and back donation between the metal, 5σ, and $2\pi^*$ orbitals within a frontier orbital framework provides a useful picture for qualitative understanding of the bonding of CO to transition metals.

Electronic excitation spectra of CO adsorbed on metal surfaces have been investigated predominantly by electron-energy-loss spectroscopy (EELS). A number of different metal surfaces have been studied, and much of this work has been summarized by Netzer *et al.*[17] and Avouris and Demuth.[18,19] On most metals two large loss bands are observed around 5–7 eV and 13–15 eV. Additional loss bands at $\approx$8.5 eV and 12 eV are reported for some systems. For weakly coupled or physisorbed CO there is general agreement, the features at 5–7 eV and $\sim$8.5 eV are due to the triplet and singlet $5\sigma\rightarrow 2\pi^*$ intramolecular CO transitions, denoted by $^3(5\sigma\rightarrow 2\pi^*)$ and $^1(5\sigma\rightarrow 2\pi^*)$, respectively. These transition energies are close to those for gas-phase CO. In addition, metal$\rightarrow$CO charge transfer (CT) transitions may also contribute to the low energy feature.[17,19] However, for chemisorbed CO there has been considerable debate over the assignment of the spectral bands, and there are broadly two interpretations. The first assigns the lower energy bands to the triplet and singlet $(5\sigma\rightarrow 2\pi^*)$ excitations, similar to physisorbed CO.[18–20] In this interpretation, the electronic excitations change only slightly with respect to the gas phase. This interpretation is supported by inverse photoemission studies,[21,22] which suggest that the $2\pi^*$ orbitals of chemisorbed CO are at lower energies than in free CO. In contrast, in an alternative view the lower energy bands are primarily due to $(d\rightarrow 2\pi^*)$ CT transitions, and the $^1(5\sigma\rightarrow 2\pi^*)$ transition is found at much higher energy and contributes to the higher energy band at 13–15 eV.[17] A number of other assignments have also been proposed for this higher energy band; these include $^1(4\sigma\rightarrow 2\pi^*)$,[23] $(1\pi\rightarrow 2\pi^*)$,[24] and to Rydberg excitations.[25]

The study of molecules adsorbed on surfaces presents a demanding challenge for theory. The large number of atoms and electrons result in the calculations being computationally intensive, and approximations to an extended surface are required. Furthermore, the presence of heavy atoms means that effects due to relativity may be important. The calculation of excited states introduces additional complexity and this is reflected in the relatively small number of papers addressing this problem. Freund *et al.*[26] used generalized valence-bond configuration-interaction (CI) calculations of NiCO to interpret EELS spectra. Excitation energies for the $^1(5\sigma\rightarrow 2\pi^*)$ transition were computed at Ni–CO distances of 1.52 and 1.65 Å. An average excitation energy of 9.9 eV was found, which was 1 eV higher than for gas-phase CO. The $^1(4\sigma\rightarrow 2\pi^*)$ transitions were calculated to lie above 11.5 eV and CT transitions were found at 8.2 eV. The weak peak at 8.5 eV was assigned to the $^1(5\sigma\rightarrow 2\pi^*)$ transition and the more intense peak at 5–7 eV to CT transitions. It was suggested that intensity borrowing into these CT transfer bands could lead to the low intensity of the $^1(5\sigma\rightarrow 2\pi^*)$ transition. The results also supported the assignment of the intense feature at $\sim$13 eV as due primarily to the $^1(4\sigma\rightarrow 2\pi^*)$ transition.

Mochizuki *et al.*[27] studied the excited states of CO adsorbed on small copper clusters. Their study used configuration interaction with single excitations (CIS). To reduce the number of configurations, those involving excitation to the virtual orbitals associated with the copper atoms were removed. This removes the intra-Cu cluster excitations and only CT excitations from cluster to CO and intra-CO excitations remain. CO adsorbed on a range of clusters of up to five atoms was studied. For the Cu(111) surface, an excitation energy of $\approx$6.5 eV was found for the $^3(5\sigma\rightarrow 2\pi^*)$ transition in the on-top binding site on a four atom cluster with two layers. For the corresponding singlet state, an excitation energy of 10 eV was reported. The $^1(4\sigma\rightarrow 2\pi^*)$ transition was calculated to lie at $\approx$12.5 eV. The $^{1,3}(1\pi\rightarrow 2\pi^*)$ excitation energies were found to lie in the region 7–10 eV; this represented a small redshift in energy and was in contrast to the $^1(5\sigma\rightarrow 2\pi^*)$ excitation energy which increased by $\approx$1.5 eV. This was attributed to a large shift in the 5σ orbital energy. It was concluded that the $^3(5\sigma\rightarrow 2\pi^*)$ and $^{1,3}(1\pi\rightarrow 2\pi^*)$ transitions would contribute to the bands at 6–7 eV and 8–10 eV, respectively, and the $^1(4\sigma\rightarrow 2\pi^*)$ transition would contribute to one of the higher lying bands. In addition, it was predicted that CT transition from Cu 3*d* orbitals would also contribute to the bands at 6–7 eV and 8–10 eV.

Nakatsuji *et al.*[28] studied the excited states of CO on a Pt surface with CIS and symmetry adapted cluster methods in order to investigate the photosimulated desorption of CO. CO was studied in the bridge binding site using a two-atom cluster model incorporating long range electrostatic forces. The interaction of CO with the surface was dominated by σ donation and π back donation and the long range effects were predicted to be less significant. Pt$\rightarrow 2\pi^*$ CT transitions were found in the 6.5–7.5 eV energy range. The calculated $^1(5\sigma\rightarrow 2\pi^*)$ excitation energy was 11.3–12.7 eV, compared to 9 eV for free CO. This represented a significant blueshift in the excitation energy.

In the approach of Klüner *et al.*,[29,30] a cluster consisting of CO and a small number of metal (Pd) atoms is embedded within a periodic DFT framework. The cluster is treated at the complete-active-space self-consistent-field (CASSCF) level with the effect of the environment included in the CASSCF calculation via a one-electron embedding potential. An excitation energy of 9.8 eV was reported for the $^1(5\sigma\rightarrow 2\pi^*)$ excitation, which was in agreement with the assignments of Avouris *et al.*[19] In the method reported by Corni and Tomasi,[31] the metal surface is treated as a continuous body that is characterized by a dielectric constant with excitation energies computed using time-dependent DFT (TDDFT) or time-dependent Hartree–Fock theory. This approach provides excitation energies of molecules close to a metal surface; however, excitation energies for CO were not reported.

We recently computed the excitation of CO adsorbed on Ni(111) within CIS and TDDFT methodologies with a small cluster model of the surface.[32] This was achieved by limiting the single excitations to include only those from the orbitals of CO. The 6-31+G* basis set was used for the carbon and oxygen atoms while the LANL2DZ (Ref. 33) basis set was used for nickel. The predicted $^1(5\sigma\rightarrow 2\pi^*)$ excitation energies were 11.19 eV and 8.66 eV for CIS and TDDFT (with the B3LYP exchange-correlation functional[34]), respectively.

TABLE I. Computed excitation energies of CO (in eV) with oscillator strengths $\geqslant 0.01$ in parentheses.

State	Transition	BLYP/6-31+G*	B3LYP/6-31+G*	B3PW91/6-31+G*	B3LYP/aug-cc-pVTZ	Expt.[a]
$a\,^3\Pi$	$^3(5\sigma\rightarrow 2\pi^*)$	5.84	5.99	5.99	6.08	6.32
$a'\,^3\Sigma^+$	$^3(1\pi\rightarrow 2\pi^*)$	7.92	8.11	8.17	8.32	8.51
$a\,^3\Delta$	$^3(1\pi\rightarrow 2\pi^*)$	8.43	8.69	8.75	8.87	9.36
	$^3(4\sigma\rightarrow 2\pi^*)$	11.17	11.75	11.82	11.84	N/A[b]
$A\,^1\Pi$	$^1(5\sigma\rightarrow 2\pi^*)$	8.28(0.12)	8.55(0.12)	8.58(0.11)	8.62(0.11)	8.51
$I\,^1\Sigma^-$	$^1(1\pi\rightarrow 2\pi^*)$	9.40	9.59	9.67	9.79	9.88
$D\,^1\Delta$	$^1(1\pi\rightarrow 2\pi^*)$	9.67	9.91	10.04	10.09	10.23
	$^1(4\sigma\rightarrow 2\pi^*)$	13.33(0.15)	13.95(0.12)	13.95(0.11)	13.92(0.11)	N/A[b]

[a]Taken from Ref. 51.
[b]N/A denotes not available.

In comparison to the corresponding excitation energies of 9.28 eV and 8.55 eV for free CO, the large blueshift in the CIS excitation energy is not observed using TDDFT. This difference in behavior was associated with the energies of the $2\pi^*$ orbitals. It has been noted in the literature previously that Hartree–Fock (HF) theory underestimates the π back donation.[35]

In this paper, we investigate the excited states of CO adsorbed on Pt(111). Using cluster models of the surface, excitation energies and oscillator strengths are computed within a TDDFT formalism. Intense CT bands are identified, and the variation of valence CO excitations to adsorption geometry and cluster size is studied. The assignment of peaks in EELS spectra is also discussed.

II. COMPUTATIONAL DETAILS

The study of the valence excitations of molecules adsorbed on transition metal surfaces within TDDFT is problematic due to the large number of electronic excitations arising from the *d* orbitals of the metal atoms. This limits the size of cluster used to model the surface to a very small number of atoms. The cost of these calculations can be reduced by limiting the possible electronic excitations to those between orbitals associated with the adsorbed molecule. Within the Tamm–Dancoff approximation,[36] excitation energies and oscillator strengths can be determined as the solutions to the eigenvalue equation[36,37]

$$\mathbf{AX} = \omega\mathbf{X}. \tag{1}$$

The matrix **A** is given by

$$A_{ai\sigma,bj\tau} = \delta_{ij}\delta_{ab}\delta_{\sigma\tau}(\varepsilon_{a\sigma} - \varepsilon_{i\tau}) + K_{ai\sigma,bj\tau}, \tag{2}$$

where **K** is the coupling matrix

$$K_{ai\sigma,bj\tau} = (\psi^*_{a\sigma}(\mathbf{r})\psi_{i\sigma}(\mathbf{r})|\psi^*_{j\tau}(\mathbf{r}')\psi_{b\tau}(\mathbf{r}')) + \int d\mathbf{r}\, d\mathbf{r}'\, \psi^*_{a\sigma}(\mathbf{r})\psi_{i\sigma}(\mathbf{r})\frac{\delta^2 E_{\mathrm{XC}}}{\delta\rho_\sigma(\mathbf{r})\,\delta\rho_\tau(\mathbf{r}')} \times \psi^*_{j\tau}(\mathbf{r}')\psi_{b\tau}(\mathbf{r}'). \tag{3}$$

The convention of $i,j,\ldots$ denoting occupied orbitals and $a,b,\ldots$ denoting virtual orbitals is adopted, while σ and τ are spin indices and $[\psi^*_{a\sigma}(\mathbf{r})\psi_{i\sigma}(\mathbf{r})|\psi^*_{j\tau}(\mathbf{r}')\psi_{b\tau}(\mathbf{r}')]$ is a two-electron integral. **X** describes the linear response of the Kohn–Sham density matrix in the basis of the unperturbed molecular orbitals, ε_i are the orbital energies, ω are the excitation energies, and E_{XC} is the exchange-correlation functional. The following equation can be solved[32]

$$\overline{\mathbf{A}}\mathbf{X} = \omega\mathbf{X}, \tag{4}$$

where

$$\overline{\mathbf{A}} = A_{\overline{ai}\sigma,\overline{bj}\tau} \tag{5}$$

and $\{\overline{i}\}$ and $\{\overline{a}\}$ are subsets of occupied and virtual orbitals, respectively. In this study, only truncation within the occupied orbital subspace is performed. $\{\overline{i}\}$ is limited to include only the seven occupied orbitals of CO (within a restricted formalism). These orbitals are selected via Mulliken populations. A parameter κ_i^{occ} is defined as

$$\kappa_i^{\mathrm{occ}} = \sum_{\overline{\lambda}} M_{\overline{\lambda i}}, \tag{6}$$

where $M_{\lambda i}$ is the contribution to the Mulliken population of orbital i from basis function λ and the summation is over basis functions centered on the carbon and oxygen atoms. Thus $M_{\lambda i}$ provides a measure of the extent to which an orbital is localized on CO. In order to select the CO occupied orbitals, only orbitals with $\kappa_i^{\mathrm{occ}} \geqslant 0.8$ a.u. are included in $\{\overline{i}\}$. The virtual orbitals of CO are more diffuse and mixed extensively with the metal orbitals; consequently, no truncation of the virtual orbitals was imposed.

In this study, the surface is modeled using finite clusters. The clusters are denoted by Pt_{m-n-o} CO where m, n, and o are the number of atoms in the first, second, and third layers, respectively. In all calculations, the cluster was treated as a singlet state. Although this may not be the ground state it should provide a reasonable model for the Pt(111) surface which is nonmagnetic. The calculation of accurate binding geometries remains a complex and ongoing problem,[12,38] and is beyond the scope of this paper. In this work, the adsorption geometries outlined by Wong and Hoffmann[1] are used. These geometries are derived from experimental data. The surface atoms are frozen in their bulk positions, with nearest neighbor distances 2.77 Å. C-metal distances are 2.23 Å, 1.85 Å, and 2.08 Å for three fold, on-top, and bridge binding sites. The C–O bond length is 1.14 Å. These geometries are in close agreement to those from DFT, which predicts C-metal distances of 2.13 Å, 1.89 Å, and 1.99 Å.[39] Furthermore, the

sensitivity of the excitation energies to the geometry is explored. For carbon and oxygen atoms the split-valence 6-31+G* Ref. 40) and correlation consistent aug-cc-pVTZ (Refs. 41 and 42) are used. The effective core potential basis set LANL2DZ (Refs. 33 and 43) is used for the platinum atoms. All calculations were performed using a development version of the Q-Chem software package.[44] For the larger clusters, to achieve more stable convergence it was necessary to ignore symmetry. Electronic spectra were simulated by representing all transitions by gaussian functions, with a bandwidth of 0.6 eV and area equivalent to the calculated intensity.

III. RESULTS AND DISCUSSION

Table I shows computed vertical excitation energies for gas phase CO for a range of methods. Where greater than 0.01, the oscillator strengths are also given. B3LYP/6-31+G* excitation energies are in good agreement with experiment. There is a larger error in the excitation energies of the triplet states. There is little difference between the excitation energies computed with the two different hybrid functionals. The predicted excitation energies are significantly better for both of the hybrid functionals than BLYP. Improving the quality of the basis set to aug-cc-pVTZ leads to a small improvement in the calculated excitation energies. Multireference configuration interaction (MRCI) calculations also provide a better description of the triplet states.[30] The quality of the basis set may be more important for Rydberg states. This will be explored in more detail later. Of primary interest in this study are the $^1(5\sigma \rightarrow 2\pi^*)$ and $^1(4\sigma \rightarrow 2\pi^*)$ transitions, since these are the only valence transition which have significant oscillator strength. The $A\,^1\Pi$ excitation energy is particularly well reproduced using B3LYP/6-31+G* and comparable to MRCI calculations.[30] Within TDDFT, the calculation of Rydberg and CT excitations is problematic. Excitations to Rydberg states are often inaccurate due to the incorrect asymptotic form of the exchange-correlation potential.[45] While the absence of nonlocal exchange introduces errors in the description of CT excitations.[46] However, we are concerned mainly with the properties of valence states. The presence of exact HF exchange in hybrid functionals such as B3LYP, leads to an improved description of Rydberg and CT excitations. In view of this, and the relatively low cost of the calculations, B3LYP/6-31+G* was used in this study.

Before examining the computed excitation energies in detail, we will discuss briefly some general features of the CO orbitals that are involved in bonding to the metal surface. These orbitals, calculated at the HF level, are depicted for the Pt_1–CO complex in Fig. 1. The 4σ and 1π orbitals remain localized on the carbon and oxygen atoms. The 1π orbital shows significant bonding between the platinum and carbon atoms. The 5σ orbital is localized on the carbon and platinum atoms. This greater interaction of the 5σ orbital with the surface is reflected in the energies of the occupied orbitals of CO. This is depicted in Fig. 2 for CO adsorbed onto different cluster models of the surface (Figs. 3–5). These energies are depicted in Fig. 5. As the CO molecule approaches the surface, at a separation of ~2.5 Å the energy of the 5σ orbital is lowered due to interaction with the *d* band. This lowering of the 5σ orbital energy increases with cluster size, but is approximately constant for the larger clusters used. The extent of this lowering is large, and for all three binding sites the 5σ orbital lies below the 1π orbitals. The lowering in energy of the 5σ orbital is estimated to be 4.4, 3.5, and 3.4 eV for the on-top, bridge, and threefold sites, respectively. This trend in the extent of interaction between the 5σ orbital and the surface for the different binding sites is consistent with the trend predicted by extended Hückel theory.[13] The effect of adsorption on the 1π orbitals is much smaller. For the threefold and bridge sites, the orbital energy is close to its gas phase value, while for the on-top site a lowering of ~0.8 eV is found. The energy of the 4σ orbital is also lowered on interaction with the surface, indicating that the 4σ orbital does play a role in

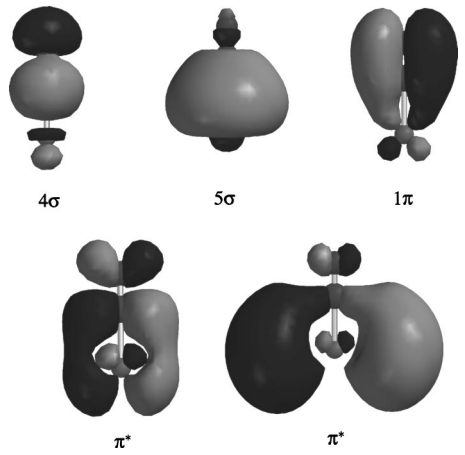

FIG. 1. Orbitals of Pt_1–CO (the lower atom is Pt).

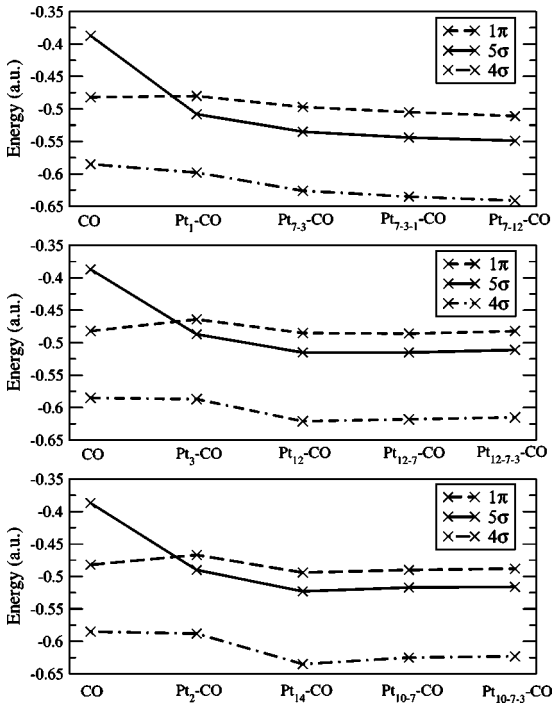

FIG. 2. Variation of the $4\sigma, 1\pi$, and 5σ orbital energies. Top panel, on-top binding site; middle panel, threefold binding site; and lower panel, bridge binding site.

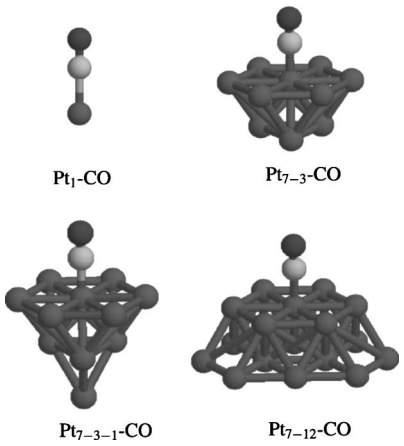

FIG. 3. Cluster models of the on-top binding site.

the bonding to the surface. Like the 5σ and 1π orbitals, the effect is greatest for the on-top site. However, the extent to which the orbital energy is lowered is much smaller than for the 5σ orbital.

In order to understand the excited states of CO adsorbed on Pt(111), it is also necessary to consider the effects of adsorption on the virtual orbitals. Earlier work has shown there to be extensive mixing of the metal and $2\pi^*$ orbitals of CO, resulting in metal-$2\pi^*$ orbitals.[8] Consequently, it becomes difficult to relate electronic transitions observed in the adsorbed CO systems with those of gas phase CO. Examination of the molecular orbitals, shows there to be more than one set of orbitals with π^* character. These π^* orbitals are also shown in Fig. 1 for the Pt_1-CO complex. For each of these orbitals there is a degenerate orbital in a perpendicular plane. The first of these orbitals has a large contribution from the carbon and oxygen atoms. This orbital corresponds to a gas-phase $2\pi^*$ CO orbital. The second π^* orbital lies predominantly on the platinum atom and has a dominant contribution from the *d* orbitals of the metal. It is useful to retain some association with the gas-phase transitions. In order to assign the orbitals of π^* character, we have evaluated the dot product of the molecular orbital coefficients of the $2\pi^*$ orbitals of gas-phase CO with the molecular orbital coefficients of the π^* orbitals in the adsorbed system

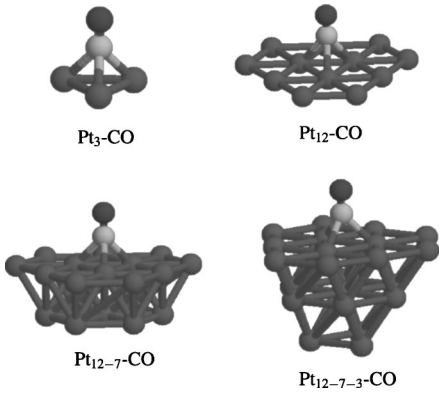

FIG. 4. Cluster models of the threefold binding site.

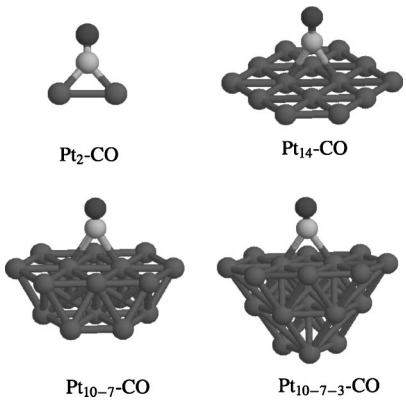

FIG. 5. Cluster models of the twofold (bridge) binding site.

$$s = \sum_{\lambda} c_{\lambda}^{\mathrm{CO}} c_{\lambda}^{\mathrm{Pt}_n\mathrm{CO}}, \tag{7}$$

where $c_{\lambda}^{\mathrm{CO}}$ and $c_{\lambda}^{\mathrm{Pt}_n\mathrm{CO}}$ are the molecular orbital coefficients of gas-phase and adsorbed CO, computed in independent calculations. This provides a rough measure of the similarity of an orbital to the $2\pi^*$ orbitals of gas-phase CO. This allows a designation of π^* orbitals associated with CO (π^*_{CO}) and those predominantly on the metal cluster (π^*_{CL}). For large clusters, the π^*_{CL} orbitals can lie much lower in energy than the $2\pi^*$ orbital of free CO. This is consistent with inverse photoemission spectroscopy studies, which predicts π^* orbitals at lower energy than the gas phase $2\pi^*$ orbitals.[47,48] Within the Blyholder model, a significant lowering in energy of the $2\pi^*$ state is not expected.[1] The appearance of π^* orbitals at lower energies reflects a breakdown of the simple Blyholder picture.

Two-electron photoemission spectroscopy has shown the $2\pi^*$ orbital to lie 3.35 eV above the Fermi level.[49] DFT with generalized gradient approximation (GGA) functionals has been shown to underestimate molecular HOMO-LUMO gaps and band gaps in semiconductors. The inclusion of HF exchange within the functional improves these properties.[50] For the $Pt_{7\text{-}3\text{-}1}$ complex, B3LYP predicts the π^*_{CO} and π^*_{CL} orbitals to lie 3.91 eV and 2.91 eV above the Fermi level, respectively. These values are consistent with the findings from experiment. The corresponding values using the BLYP functional, which is a GGA functional and does not contain HF exchange, are 0.6 eV and 2.5 eV. Thus it can be seen clearly that the hybrid functionals lead to a significant improvement in the description of the π^* states.

A. On-top binding site

For small clusters it is possible to calculate excitation energies with traditional TDDFT. This provides an opportunity to study intrametal and CT excitations, in addition to examining the error introduced through limiting the electronic excitations. Computed excitation energies for Pt_1-CO are shown in Table II. Initially, we will discuss results obtained when no restriction of the electronic excitations is imposed. It is not possible to report all of the extremely large number of intrametal and CT electronic transitions. Consequently, only valence excitations along with the transitions with greatest intensity are reported. The region of the spec-

TABLE II. Computed excitation energies of Pt_1–CO (in eV) with nonzero oscillator strengths in parentheses. Basis sets refer to the carbon and oxygen atoms. Only valence and transitions with greatest intensity are shown for the B3LYP calculation with no restriction. *R* denotes a Rydberg orbital and *r*B3LYP denotes a calculation in which restriction of the single excitation space has been imposed.

Transition	B3LYP/aug-cc-pVTZ	B3LYP/6-31+G*	*r*B3LYP/6-31+G*
$^1(d\rightarrow\pi^*_{CO})$	4.50(0.14)	4.48(0.14)	
$^1(d\rightarrow\pi^*_{CL})$	6.47(0.21)	6.48(0.21)	
$^1(d\rightarrow\pi^*_{CL})$	6.52(0.22)	6.51(0.12)	
$^1(d\rightarrow R_\sigma)$	7.08(0.04)	6.95(0.09)	
$(a'\,^3\Sigma^+)^3(1\pi\rightarrow\pi^*_{CO})$	8.44	8.41	8.44
$(d\,^3\Delta)^3(1\pi\rightarrow\pi^*_{CO})$	8.96	8.94	8.96
$(I\,^1\Sigma^-)^1(1\pi\rightarrow\pi^*_{CO})$	9.69	9.68	9.68
$(D\,^1\Delta)^1(1\pi\rightarrow\pi^*_{CO})$	9.94	9.93	9.93
$(a\,^3\Pi)^3(5\sigma\rightarrow\pi^*_{CO})$	10.00	10.04	10.03
$^1(5\sigma\rightarrow R_\sigma)$	10.79(0.49)	10.51(0.21)	10.47(0.38)
$(A\,^1\Pi)^1(5\sigma\rightarrow\pi^*_{CO})$	11.04(0.16)	11.13(0.26)	10.91(0.01)
$^1(4\sigma\rightarrow R_\sigma)$	12.85(1.05)	12.71(0.92)	12.50(0.25)
$^1(1\pi\rightarrow\pi^*_{CL})$	12.67	12.67	12.64
$^1(5\sigma\rightarrow\pi^*_{CL})$	13.35(0.08)	13.40(0.02)	13.40(0.02)
$^1(4\sigma\rightarrow\pi^*_{CO})$	14.38(0.16)	14.14(0.20)	14.13(0.16)
$^3(4\sigma\rightarrow\pi^*_{CL})$	15.57	15.63	15.63
$^1(4\sigma\rightarrow\pi^*_{CL})$	16.18(0.04)	16.23(0.03)	16.27(0.04)
Time (s)	638	370	161

trum up to 3.5 eV is dominated by weak singlet and triplet transitions from the Pt *d* orbitals to a Rydberg orbital of σ character (not shown). At higher energies a large number of $d\rightarrow\pi^*$ transitions are observed. Many of these have large oscillator strength. The most intense of these are calculated to lie at 4.48 eV, 6.48 eV, and 6.51 eV. The transition at 4.48 eV corresponds to excitation to the π^* orbitals that most closely resemble the $2\pi^*$ orbitals of gas-phase CO. The higher energy transitions correspond to excitations to other orbitals of π^* character, and have been denoted by π^*_{CL}. At 6.95 eV are further $^1(d\rightarrow R_\sigma)$ transitions with significant intensity, where *R* denotes a Rydberg orbital.

The valence $(1\pi\rightarrow\pi^*_{CO})$ excitations lie between 8.5 and 10 eV. The state labels are included to allow comparison with the corresponding excitations in gas-phase CO. In contrast to gas phase, the $(1\pi\rightarrow\pi^*_{CO})$ transitions lie below the $(5\sigma\rightarrow\pi^*_{CO})$ transitions. This is a consequence of the lowering of the 5σ orbital below the 1π orbital on adsorption. The $^3(1\pi\rightarrow\pi^*_{CO})$ excitations show a small blueshift, while the corresponding singlet excitations are close to their gas-phase counterparts. This is not surprising since in Pt_1–CO both 1π and π^*_{CO} orbital energies are close to their gas-phase values. The calculations of Mochizuki *et al.*,[27] also predicted $(1\pi\rightarrow\pi^*)$ excitations between 7–10 eV, however, a redshift in the excitation energies with respect to gas phase was observed.

The lowering of the 5σ orbital energy in conjunction with the π^*_{CO} orbital energy remaining constant, should lead to a large blueshift in the $(5\sigma\rightarrow\pi^*_{CO})$ excitation energies. The $^3(5\sigma\rightarrow\pi^*_{CO})$ and $^1(5\sigma\rightarrow\pi^*_{CO})$ excitation energies are computed to be 10.04 eV and 11.13 eV, respectively. This represents blueshifts of 4.05 eV and 2.58 eV. The $^3(5\sigma\rightarrow\pi^*_{CO})$ excitation energy is reported to be 6 eV from experiment.[26] Since this transition is very weak, accurate determination of its value from experiment is difficult. Although the singlet-triplet splitting has been found to decrease on adsorption,[26] the calculated blueshift appears too large. A smaller blueshift is computed for the $^1(5\sigma\rightarrow\pi^*_{CO})$ transition. However, the shift is larger than the shifts found in previous studies.[26,27] The triplet and singlet $4\sigma\rightarrow\pi^*_{CO}$ transitions are predicted to undergo a small blueshift and redshift, respectively. At higher energies lie further excitations to virtual orbitals of π^* character. These orbitals are predominantly located on the Pt atom and are denoted by π^*_{CL} The intensities of the valence excitations are low, except for the $^1(4\sigma\rightarrow\pi^*_{CO})$ and $^1(5\sigma\rightarrow\pi^*_{CO})$ excitations which are predicted to have significant intensity. This is similar to gas-phase CO.

In addition to the valence excitations, a large number of excitations from the $4\sigma, 1\pi$, and 5σ orbitals to Rydberg orbitals are observed. In particular, intense transitions from the 4σ and 5σ orbitals to a Rydberg orbital of σ character are computed to lie at 12.71 eV and 10.51 eV. Table II also contains excitation energies computed with the better quality aug-cc-pVTZ basis set for the carbon and oxygen atoms. In general, there is good agreement between the values computed with the smaller basis set and a similar picture of the spectrum is obtained. Larger deviations occur to excitations to Rydberg orbitals, this arises due to the presence of more diffuse functions in the aug-cc-pVTZ basis set. We have not explored the sensitivity of the excitation energies to the quality of the platinum basis set.

Overall, calculations on the Pt_1–CO complex show there to be low-lying $d\rightarrow\pi^*$ excitations and some intense Rydberg transitions at higher energies. The $^{1,3}(1\pi\rightarrow\pi^*_{CO})$ excitation energies are close to their gas phase values, but there is a large blue-shift for the $^{1,3}(5\sigma\rightarrow\pi^*_{CO})$ excitations. However, the Pt_1–CO complex is unlikely to provide an accurate representation of the electronic structure of CO adsorbed onto the Pt(111) surface. Consequently, it is necessary to study CO adsorbed on larger cluster models of the metal surface.

TABLE III. Variation of computed excitation energies (in eV) with cluster size for the on-top binding site.

Transition	Pt_1-CO	$Pt_{7-3}-CO$	$Pt_{7-3-1}-CO$
$^1(5\sigma\rightarrow\pi^*_{CL})$	13.40	10.06	10.39
$^1(5\sigma\rightarrow\pi^*_{CO})$	10.91	11.70	11.77
$^1(1\pi\rightarrow\pi^*_{CL})$	12.64	9.03	9.34
$^1(1\pi\rightarrow\pi^*_{CO})$	9.68	10.50	10.58
$^1(4\sigma\rightarrow\pi^*_{CL})$	16.27	12.47	12.80
$^1(4\sigma\rightarrow\pi^*_{CO})$	14.13	14.89	14.96
$^1(5\sigma\rightarrow R_\sigma)$	10.47	10.27	10.30
$^1(4\sigma\rightarrow R_\sigma)$	12.50	12.64	12.76

Table II also shows the computed excitation energies when the single excitation space is restricted to include only excitations from the seven occupied CO orbitals, these calculations are denoted by *r*B3LYP. Within this scheme, the low-lying ($d\rightarrow\pi^*$) excitations are no longer observed. Imposing this restriction will introduce an error. For most of the excitations, this error is small. Larger errors are observed for the $^1(5\sigma\rightarrow\pi^*_{CO})$ and $^1(4\sigma\rightarrow\pi^*_{CO})$ transitions. This is due to strong mixing with excitations involving *d* orbitals. The removal of this mixing also leads to a reduction in intensity. This mixing is particularly large for the on-top binding site, which represents a worst case scenario for the truncation scheme. Much smaller errors are observed for these excitations for the threefold and bridge binding sites (see later). The advantage of the truncated scheme is illustrated by the time for the calculations. Imposing the truncation reduces the time for the calculation by over a factor of two. These timings refer to calculations on a PC with a 2.0 GHz processor and 1 GB of memory. The extent to which the cost is reduced will grow as the size of cluster is increased. Consequently, within this approach it is possible to study the excitation energies on larger cluster models of the surface.

Table III shows the computed singlet valence and intense Rydberg excitations using larger clusters to model the surface. These clusters lead to a different picture of the excited states. For the larger clusters there are low-lying π^* orbitals. Evaluation of the dot product of these orbitals with gas-phase CO $2\pi^*$ orbitals [Eq. (7)] yields a value of ~0.1. This is in comparison to ~0.7 for the π^* orbitals of higher energy. Thus for the larger clusters there are π^*_{CL} orbitals of low energy, while the π^*_{CO} orbitals lie only slightly lower than the $2\pi^*$ orbitals of gas-phase CO. There is an increase in the $^1(5\sigma\rightarrow\pi^*_{CO})$ excitation energy. This is due to the lower 5σ orbital energy in the larger clusters (see Fig. 2). The appearance of low-lying π^*_{CL} orbitals leads to a large decrease in the $^1(5\sigma\rightarrow\pi^*_{CL})$ excitation energy. This transition lies ≈1.8 eV above the gas phase $^1(5\sigma\rightarrow 2\pi^*)$ excitation energy. This shift is closer to the value reported by Mochizuki *et al.*[27]

If the BLYP exchange correlation functional is used, the predicted excitation energies are considerably smaller than for B3LYP. For the $^1(5\sigma\rightarrow\pi^*_{CL})$ and $^1(5\sigma\rightarrow\pi^*_{CO})$ excitations, values of 8.80 eV and 11.03 eV are obtained. These are 1.59 eV and 0.74 eV below the B3LYP values. Similarly the BLYP transition energies for the $^1(1\pi\rightarrow\pi^*_{CL})$ and $^1(1\pi\rightarrow\pi^*_{CO})$ excitations are 7.91 eV and 9.82 eV, these are 1.43 eV and 0.70 eV below the B3LYP values. This difference between the two functionals arises from the underestimation of the band gap by BLYP.

On larger clusters, a lowering of the 1π orbital leads to an increase in the $^1(1\pi\rightarrow\pi^*_{CO})$ excitation energies. The $^1(1\pi\rightarrow\pi^*_{CL})$ transitions appear in the range 9–9.4 eV, this represents a redshift with respect to the gas-phase $^1(1\pi\rightarrow 2\pi^*)$ transitions. The $^1(4\sigma-\pi^*_{CO})$ transition remains at high energy, while the $^1(4\sigma\rightarrow\pi^*_{CL})$ transition is computed to lie at 12.8 eV. This is close to the value of 12.5 eV reported by Mochizuki *et al.*[27] There is a small decrease in the computed $^1(5\sigma\rightarrow R_\sigma)$ and $^1(4\sigma\rightarrow R_\sigma)$ excitation energies. This is probably due to the lowering of the 4σ and 5σ orbital energies. However, this is partially offset by a stabilization of the R_σ orbital. There is also a decrease in the intensity of the $^1(4\sigma\rightarrow R_\sigma)$ transition.

B. Threefold binding site

The smallest model of the threefold binding site is Pt_3-CO. Table IV shows the calculated excitation energies of Pt_3-CO, with and without truncation of the single excitation space. Again, for the calculations with no restriction, only the transitions with the greatest intensity are reported. The low energy region of the spectrum is dominated by singlet and triplet $d\rightarrow\pi^*$ and $d\rightarrow$Rydberg transitions. Many of these have substantial oscillator strength. The most intense of these are calculated to lie at 6.15 eV, ~6.5 eV, and 7.08 eV. These intense transitions are mixed to a large extent, but are predominantly $d\rightarrow\pi^*$.

The low-lying valence excitations lie between 7.8 and 8.8 eV. These transitions correspond to excitation to a π^* orbital which is significantly lower in energy than the gas-phase CO $2\pi^*$ orbitals. Dot product analysis gives a value of $s\approx 0.1$, consequently, these orbitals have been labeled π^*_{CL}. The $^1(5\sigma\rightarrow\pi^*_{CL})$ excitation energy is computed to be 8.75 eV, this is close to 8.66 eV reported for Ni(111).[32] This represents a small blueshift relative to free CO of 0.2 eV. The corresponding triplet state is found at 8.56 eV. Similar to the on-top site, this is higher than the value reported in experiment. The $^{1,3}(1\pi\rightarrow\pi^*_{CL})$ excitations are all lowered relative to free CO. In particular, the singlet states undergo large redshifts. The calculations indicate that these transitions occur at significantly lower energy than for the on-top binding site. This difference is due to the 5σ and 1π orbitals being higher in energy when CO occupies the threefold site. It should be noted that, in addition to the valence transitions, there are also many excitations from *d* orbitals of the metal in the energy range 8–9 eV. Some of these transitions do have a significant intensity and are only not included in Table IV because of their large numbers. It is probably because of these excitations, and the relatively low intensity of the valence excitations that their assignment has been problematic.

At higher energies are further $^1(d\rightarrow R)$ and π^* excitations. These higher energy π^* orbitals have $s\approx 0.5$, and have been denoted π^*_{CO}. The $^1(5\sigma\rightarrow\pi^*_{CO})$ lies at 11.18 eV with an oscillator strength of 0.09. This represents a large blueshift of 2.63 eV relative to the $^1(5\sigma\rightarrow 2\pi^*)$ gas-phase transition and reflects the decrease in energy of the 5σ orbital. In addition,

TABLE IV. Computed excitation energies of Pt_3–CO (in eV) with oscillator strengths $\geqslant 0.01$ in parentheses. Only valence and transitions with greatest intensity are shown. *R* denotes a Rydberg orbital and *r*B3LYP denotes a calculation in which restriction of the single excitation subspace is imposed.

Transition	B3LYP	*r*B3LYP	Transition	B3LYP	*r*B3LYP
$^1(d\rightarrow\pi^*_{CL})$	6.15(0.19)		$^1(1\pi\rightarrow\pi^*_{CO})$	10.22	10.18
$^1(d\rightarrow R)$	6.15(0.26)		$^1(d\rightarrow R)$	10.31(0.22)	
$^1(d\rightarrow\pi^*_{CO})$	6.15(0.18)		$^1(d\rightarrow R)$	10.31(0.28)	
$^1(d\rightarrow\pi^*_{CL})$	6.48(0.16)		$^1(1\pi\rightarrow\pi^*_{CO})$	10.38	10.39(0.01)
$^1(d\rightarrow\pi^*_{CL})$	6.49(0.17)		$^1(d\rightarrow R)$	10.47(0.17)	
$^1(d\rightarrow R)$	7.08(0.18)		$^3(5\sigma\rightarrow\pi^*_{CO})$	10.59	10.56
$^3(1\pi\rightarrow\pi^*_{CL})$	7.78	7.74	$^1(5\sigma\rightarrow\pi^*_{CO})$	11.18(0.09)	11.19(0.02)
$^3(1\pi\rightarrow\pi^*_{CL})$	7.90	7.87	$^1(d\rightarrow R)$	11.22(0.17)	
$^1(1\pi\rightarrow\pi^*_{CL})$	8.01	8.00	$^3(4\sigma\rightarrow\pi^*_{CL})$	11.22	11.22
$^1(1\pi\rightarrow\pi^*_{CL})$	8.03	8.05	$^1(4\sigma\rightarrow\pi^*_{CL})$	11.49(0.09)	11.47(0.06)
$^3(5\sigma\rightarrow\pi^*_{CL})$	8.56	8.54	$^1(5\sigma\rightarrow R)$	11.49(0.01)	11.60(0.05)
$^1(5\sigma\rightarrow\pi^*_{CL})$	8.75(0.01)	8.75(0.05)	$^1(4\sigma\rightarrow R)$	12.02(0.05)	12.04(0.23)
$^1(d\rightarrow R)$	9.28(0.24)		$^1(d\rightarrow R)$	12.91(0.14)	
$^1(d\rightarrow R)$	9.28(0.16)		$^3(4\sigma\rightarrow\pi^*_{CO})$	13.17	13.14
$^3(1\pi\rightarrow\pi^*_{CO})$	9.33	9.33	$^1(d\rightarrow R)$	13.74(0.15)	
$^1(5\sigma\rightarrow R)$	9.53(0.03)	9.56(0.23)	$^1(4\sigma\rightarrow\pi^*_{CO})$	14.59(0.10)	14.51(0.03)
$^3(1\pi\rightarrow\pi^*_{CO})$	9.69	9.65			
Time (s)				9116	1490

the $^1(4\sigma\rightarrow\pi^*_{CL})$ transition is computed to lie at 11.49 eV with an oscillator strength of 0.09 and the $^1(4\sigma\rightarrow\pi^*_{CO})$ transition at 14.59 eV. This compares with the gas-phase $^1(4\sigma\rightarrow 2\pi^*)$ transition which lies at 13.95 eV (0.12). The energy of the 4σ orbital undergoes little change on adsorption and like the corresponding excitation from the 1π orbital, redshifts and blueshifts relative to the gas-phase excitations are observed for excitations to π^*_{CL} and π^*_{CO} orbitals, respectively.

Introducing the restriction of the electronic excitations introduces an error into the predicted excitation energies of less than 0.05 eV. The computed oscillator strengths are more sensitive to the truncation. There is an increase in the oscillator strength for the $^1(5\sigma\rightarrow\pi^*_{CL})$ transition. This may reflect a reduction in intensity borrowing by the CT transitions, since many of these transitions are no longer present. An increase in intensity is also observed for $^1(5\sigma\rightarrow R)$ and $^1(4\sigma\rightarrow R)$ transitions. Both of these transitions correspond to excitation to the lowest lying Rydberg orbital. This orbital is located predominantly on the metal atoms, giving CT character to the transitions. For this larger cluster, the computational benefit of the truncation scheme is more clear. The time for the TDDFT calculation is reduced by approximately a factor of 6.

The larger cluster models lead to an increase in the predicted excitation energies. The $^1(5\sigma\rightarrow\pi^*_{CO})$ excitation energy is estimated to be 11.66 eV. This is a blueshift of 2.11 eV relative to the gas phase (see Table V). This shift is smaller than the corresponding shift for the on-top binding site. The $^1(1\pi\rightarrow\pi^*_{CO})$ transition lies 1.15 eV above its gas-phase value. For the $Pt_{12\text{-}7}$–CO complex, calculation of the $^1(4\sigma\rightarrow\pi^*_{CO})$ and $^1(4\sigma\rightarrow\pi^*_{CL})$ excitation energies was not possible with our current computational resources. However, for the Pt_{12}–CO complex the $^1(4\sigma\rightarrow\pi^*_{CO})$ is lower than for the on-top binding site and blueshifted relative to the gas phase. Excitation to π^* orbitals of π^*_{CL} character lie lower in energy.

C. Twofold (bridge) binding site

Table VI shows the computed excitation energies for Pt_2–CO, where CO occupies the bridge binding site. For this site, there is a significant split in the degeneracy of the π orbitals. If the Pt–Pt and C–O bonds lie on the *x* and *z* axis, respectively, then the occupied π_x orbital lies below the π_y. For the antibonding orbitals, this order is reversed with the π^*_y being lower in energy.

The calculation shows a number of intense $^1(d\rightarrow R)$ and $^1(d\rightarrow\pi^*)$ transitions. The most intense of these is computed to lie at 5.84 eV, 10.51 eV, and 12.82 eV. The most intense valence transition are predicted to be the $^1(5\sigma\rightarrow\pi^*_{CO,x})$ and $^1(4\sigma\rightarrow\pi^*_{CO,y})$ excitations. These transitions lie at 11.36 eV and 13.99 eV, respectively. Similar to the other binding sites, the restriction of the single excitation space introduces a relatively small error but leads to substantial computational savings.

For the larger clusters the energy difference between the π orbitals in the *x* and *y* directions is much smaller. The difference between the corresponding excitation energies is also reduced (Table VII). Similar to the on-top binding site, there is a large decrease in the energy for excitation to the π^*_{CL} orbitals when larger clusters are used. The predicted $^1(5\sigma\rightarrow\pi^*_{CO})$ excitation energies of 11.16 eV and 11.48 eV are consistent with the work of Nakatsuji *et al.* who pre-

TABLE V. Variation of computed excitation energies (in eV) with cluster size for the threefold binding site.

Transition	Pt_3–CO	Pt_{12}–CO	$Pt_{12\text{-}7}$–CO
$^1(5\sigma\rightarrow\pi^*_{CL})$	8.75	10.17	9.20
$^1(5\sigma\rightarrow\pi^*_{CO})$	11.19	11.49	11.66
$^1(1\pi\rightarrow\pi^*_{CL})$	8.00	9.18	8.39
$^1(1\pi\rightarrow\pi^*_{CO})$	10.18	10.43	10.74
$^1(4\sigma\rightarrow\pi^*_{CL})$	11.47	13.17	⋯
$^1(4\sigma\rightarrow\pi^*_{CO})$	14.51	14.70	⋯

TABLE VI. Computed excitation energies of Pt_2–CO (in eV) with oscillator strengths in parentheses. The Pt–Pt and Pt–C bonds lie along the *x* and *z* axes, respectively. Only valence and transitions with the greatest intensity are shown. *R* denotes a Rydberg orbital and *r*B3LYP denotes a calculation in which restriction of the single excitation subspace is imposed.

Transition	B3LYP	*r*B3LYP	Transition	B3LYP	*r*B3LYP
$^1(d\rightarrow R_\sigma)$	5.77(0.12)		$^1(4\sigma\rightarrow R)$	12.04(0.13)	12.01(0.26)
$^1(d\rightarrow \pi^*_{\mathrm{CL},y})$	5.84(0.47)		$^3(1\pi_x\rightarrow \pi^*_{\mathrm{CL},y})$	12.06	12.05
$^1(d\rightarrow \pi^*_{\mathrm{CL},x})$	6.92(0.22)		$^1(1\pi_x\rightarrow \pi^*_{\mathrm{CL},y})$	12.18	12.18
$^1(d\rightarrow \pi^*_{\mathrm{CL},y})$	7.75(0.12)		$^3(4\sigma\rightarrow \pi^*_{\mathrm{CO},y})$	12.23	12.22
$^3(1\pi_y\rightarrow \pi^*_{\mathrm{CO},y})$	8.30	8.35	$^1(d\rightarrow R)$	12.42(0.42)	
$^3(1\pi_x\rightarrow \pi^*_{\mathrm{CO},y})$	9.27	9.26	$^3(5\sigma\rightarrow \pi^*_{\mathrm{CL},y})$	12.45	12.45
$^3(5\sigma\rightarrow \pi^*_{\mathrm{CO},y})$	9.75	9.77	$^3(1\pi_y\rightarrow \pi^*_{\mathrm{CL},x})$	12.58	12.57
$^1(1\pi_x\rightarrow \pi^*_{\mathrm{CO},y})$	9.79	9.81	$^1(1\pi_y\rightarrow \pi^*_{\mathrm{CL},x})$	12.59	12.58
$^1(d\rightarrow R)$	9.86(0.19)		$^1(5\sigma\rightarrow \pi^*_{\mathrm{CL},y})$	12.71(0.01)	12.70(0.02)
$^3(1\pi_x\rightarrow \pi^*_{\mathrm{CO},x})$	9.91	9.96	$^1(d\rightarrow R)$	12.82(0.46)	
$^3(1\pi_y\rightarrow \pi^*_{\mathrm{CO},x})$	10.05	10.05	$^3(1\pi_x\rightarrow \pi^*_{\mathrm{CL},x})$	12.92	12.92
$^1(1\pi_y\rightarrow \pi^*_{\mathrm{CO},y})$	10.20(0.01)	10.20(0.14)	$^1(1\pi_x\rightarrow \pi^*_{\mathrm{CL},x})$	12.96	12.97
$^1(1\pi_y\rightarrow \pi^*_{\mathrm{CO},x})$	10.28	10.31	$^3(4\sigma\rightarrow \pi^*_{\mathrm{CO},x})$	13.34	13.35
$^1(d\rightarrow R)$	10.48(0.19)		$^3(5\sigma\rightarrow \pi^*_{\mathrm{CL},x})$	13.37	13.38
$^1(d\rightarrow R)$	10.51(0.42)		$^1(5\sigma\rightarrow \pi^*_{\mathrm{CL},x})$	13.39(0.02)	13.39(0.02)
$^1(5\sigma\rightarrow \pi^*_{\mathrm{CO},y})$	10.59	10.56(0.01)	$^1(4\sigma\rightarrow \pi^*_{\mathrm{CO},y})$	13.99(0.33)	13.86(0.14)
$^3(5\sigma\rightarrow \pi^*_{\mathrm{CO},x})$	10.71	10.71	$^1(4\sigma\rightarrow \pi^*_{\mathrm{CO},x})$	14.66(0.03)	14.64(0.05)
$^1(1\pi_x\rightarrow \pi^*_{\mathrm{CO},x})$	10.91	10.97	$^3(4\sigma\rightarrow \pi^*_{\mathrm{CL},y})$	15.04	15.04
$^1(d\rightarrow R)$	10.91(0.22)		$^1(4\sigma\rightarrow \pi^*_{\mathrm{CL},y})$	15.81(0.03)	15.89(0.05)
$^1(5\sigma\rightarrow \pi^*_{\mathrm{CO},x})$	11.36(0.16)	11.33(0.07)	$^3(4\sigma\rightarrow \pi^*_{\mathrm{CL},x})$	16.03	16.03
$^3(1\pi_y\rightarrow \pi^*_{\mathrm{CL},y})$	11.52	11.49	$^1(4\sigma\rightarrow \pi^*_{\mathrm{CL},x})$	16.11(0.02)	16.11(0.01)
$^1(1\pi_y\rightarrow \pi^*_{\mathrm{CL},y})$	11.54(0.06)	11.53(0.01)			
Time (s)				2611	765

dicted these transitions to lie between 11.3 and 12.7 eV. The $^1(1\pi\rightarrow\pi^*_{\mathrm{CL}})$ transitions are calculated to lie between 9 and 9.5 eV, while the $^1(1\pi\rightarrow\pi^*_{\mathrm{CO}})$ transitions are higher in energy between 10.1 and 10.6 eV. Excitations from the 4σ orbital are computed to lie above ≈13 eV.

D. Changes in adsorption geometry

Predicted excitation energies do depend on the size of the cluster. Since the determination of accurate binding geometries is difficult, it is informative to study the sensitivity of the computed excitation energies to small variations in the binding geometry. Computed excitation energies for the $Pt_{7\text{-}3\text{-}1}$–CO complex with varying Pt–C bond length are shown in Table VIII. A Pt–C bond length of 1.85 Å corresponds to the experimental structure. For the $^1(5\sigma\rightarrow\pi^*_{\mathrm{CL}})$ and $^1(5\sigma\rightarrow R_\sigma)$ excitations, there is a decrease in the excitation energy as CO moves closer or further from the surface. This arises from a destabilization of the 5σ orbital. Since the 5σ orbital is dominant in the bonding to the metal surface, it is likely to be at its most stable in the optimum binding configuration. Consequently, changes in this geometry will lead to a destabilization. This is consistent with the results of Freund *et al.*,[26] where smaller shifts in the $^1(5\sigma\rightarrow\pi^*_{\mathrm{CL}})$ excitation energies in calculations of Pt_1–CO were predicted. However, Pt–C bond lengths smaller than those used in the calculations of Pt_1–CO described in this paper were considered. For the $^1(5\sigma\rightarrow\pi^*_{\mathrm{CO}})$ excitation a different trend is observed. For this transition there is a consistent increase in the excitation energy with decreasing Pt–C distance. As CO becomes closer to the surface, there is a significant destabilization of the π^*_{CO} orbital energy. At short $R_{\mathrm{Pt–C}}$ this dominates the destabilization of the 5σ orbital leading to a blueshift. A different behavior is observed for the the 4σ orbital. There is a large stabilization of the 4σ orbital at shorter $R_{\mathrm{Pt–C}}$, leading to an increase in the corresponding excitation energies. In general, there is an increase in the $^1(1\pi\rightarrow\pi^*)$ excitations as the Pt–C distance is lengthened or shortened. In part, this arises from a small stabilization of the 1π orbitals.

TABLE VII. Variation of computed excitation energies (in eV) with cluster size for the bridge binding site.

Transition	Pt_2–CO	Pt_{14}–CO	$Pt_{10\text{-}7}$–CO
$^1(5\sigma\rightarrow \pi^*_{\mathrm{CL},y})$	12.70	10.33	10.04
$^1(5\sigma\rightarrow \pi^*_{\mathrm{CL},x})$	13.39	10.36	10.18
$^1(5\sigma\rightarrow \pi^*_{\mathrm{CO},y})$	10.59	11.56	11.16
$^1(5\sigma\rightarrow \pi^*_{\mathrm{CO},x})$	11.36	11.72	11.48
$^1(1\pi_x\rightarrow \pi^*_{\mathrm{CL},y})$	12.96	9.32	9.05
$^1(1\pi_x\rightarrow \pi^*_{\mathrm{CL},x})$	12.18	9.74	9.28
$^1(1\pi_x\rightarrow \pi^*_{\mathrm{CO},y})$	9.79	10.55	10.17
$^1(1\pi_x\rightarrow \pi^*_{\mathrm{CO},x})$	10.91	10.76	10.49
$^1(1\pi_y\rightarrow \pi^*_{\mathrm{CL},y})$	10.54	9.49	9.40
$^1(1\pi_y\rightarrow \pi^*_{\mathrm{CL},x})$	12.59	9.32	9.47
$^1(1\pi_y\rightarrow \pi^*_{\mathrm{CO},y})$	9.98	10.76	10.50
$^1(1\pi_y\rightarrow \pi^*_{\mathrm{CO},x})$	10.28	10.74	10.59
$^1(4\sigma\rightarrow \pi^*_{\mathrm{CL},y})$	15.81	13.40	12.97
$^1(4\sigma\rightarrow \pi^*_{\mathrm{CL},x})$	16.11	13.47	13.05
$^1(4\sigma\rightarrow \pi^*_{\mathrm{CO},y})$	13.99	15.19	⋯
$^1(4\sigma\rightarrow \pi^*_{\mathrm{CO},x})$	14.66	15.21	⋯

TABLE VIII. Variation of computed excitation energies (in eV) with the carbon-surface distance for the on-top binding site of the $Pt_{7\text{-}3\text{-}1}$–CO complex.

Transition	$R_{Pt-C}=1.55$	$R_{Pt-C}=1.75$	$R_{Pt-C}=1.85$	$R_{Pt-C}=1.95$	$R_{Pt-C}=2.15$
$^1(5\sigma\rightarrow\pi^*_{CL})$	9.87	10.23	10.39	10.30	9.82
$^1(5\sigma\rightarrow\pi^*_{CO})$	12.06	11.90	11.77	11.61	11.10
$^1(1\pi\rightarrow\pi^*_{CL})$	9.55	9.19	9.34	9.45	9.64
$^1(1\pi\rightarrow\pi^*_{CO})$	11.66	10.73	10.58	10.61	10.77
$^1(4\sigma\rightarrow\pi^*_{CL})$	13.84	13.01	12.80	12.65	12.59
$^1(4\sigma\rightarrow\pi^*_{CO})$	16.38	15.52	14.96	14.77	14.26
$^1(5\sigma\rightarrow R_\sigma)$	10.05	10.21	10.30	10.17	9.55
$^1(4\sigma\rightarrow R_\sigma)$	13.81	12.86	12.19	12.01	12.05

E. Simulation of electronic spectrum

Figure 6 shows experimental EELS spectra and a simulated spectrum. The experimental spectrum depicted by the solid line is of CO adsorbed on the Ni(100) surface.[23] This spectrum has been used because it shows four resolved peaks. The second spectrum of CO on the Pt(111) surface shows only two peaks at 5–7 eV and 13–15 eV.[24] This is common for the EELS spectra of CO on many transition metal surfaces. The theoretical spectrum has been computed using the Pt_7–CO cluster with electronic excitations from the occupied orbitals of the carbon, oxygen and the central platinum atoms included within the singles excitation space. The theoretical spectrum also shows four peaks. The majority of the intensity of the peak at 5.7 eV arises from a $^1(d\rightarrow R)$ excitation. This peak is much weaker than in experiment. In the calculation only excitations from the *d* orbitals of one Pt atom are included. If excitations from additional Pt atoms are included, then more intense $^1(d\rightarrow\pi^*)$ excitations are observed and this peaks becomes more intense. This also has the effect of "washing out" the peak at 8.5 eV. This is presumably why in many EELS spectra where the 8.5 eV peak is not present. The band at 8.5 eV has contributions from several $^1(d\rightarrow R)$ and $^1(d\rightarrow\pi^*)$ excitations. The band at 10.8 eV is due primarily to a $^1(5\sigma\rightarrow R)$ transition, with the remaining band arising from $^1(d\rightarrow R)$ and $^1(1\pi\rightarrow\pi^*)$ excitations. $^1(5\sigma\rightarrow\pi^*)$ and $^1(4\sigma\rightarrow\pi^*)$ excitations also contribute to these bands.

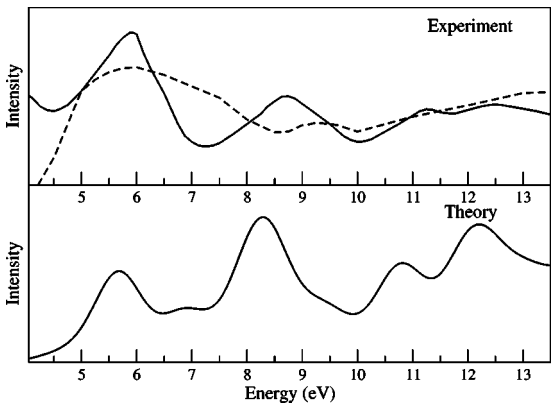

FIG. 6. Theoretical and experimental spectra. Solid line represents experimental spectrum of CO on Ni(100) (Ref. 23) and broken line represents experimental spectrum of CO on Pt(111) (Ref. 24).

IV. CONCLUSIONS

The calculation of the excited states of molecules adsorbed on transition metal surfaces presents a difficult challenge for theory. In this paper, we have described a method through which this can be achieved. While errors in the calculations remain, they are sufficiently accurate to make qualitative predictions with some confidence. This method has been applied in a detailed study of the electronic excitations of CO on the Pt(111) surface. The excited states of CO in the on-top, threefold, and bridge binding sites have been calculated and variations arising from changes in the binding geometry explored. In previous work,[8] it has been observed that there is significant mixing between the CO and metal orbitals. Consequently, it becomes difficult to interpret the results in terms of the excitations in gas phase CO. However, it is useful to retain some association with the gas-phase picture since this provides insight into the electronic structure changes that occur on adsorption. Using a dot product analysis of the molecular orbital coefficients, the π^* orbitals that most closely resemble those of CO can be identified. This allows the orbitals to the loosely classified π^*_{CO} or π^*_{CL}. This analysis shows that the π^*_{CO} orbitals remain slightly lowered in energy after adsorption. At lower energy are further orbitals of π^* character which are associated predominantly with the metal atoms of the cluster. This interpretation is consistent with the detection of low energy π^* orbitals in inverse photoemission studies[21,22] and the prediction within the Blyholder model that the CO orbitals are not lowered to a significant extent. Furthermore, the B3LYP functional predicts a Fermi level $-\pi^*$ energy separation that is in agreement with experiment. The corresponding gap predicted by the BLYP functional is too small.

The results of this study are consistent with previous work. The calculations find intense $^1(d\rightarrow R)$ and $^1(d\rightarrow\pi^*)$ excitations in between 5–7 eV. For the on-top site, our calculations predict a blueshift of $\approx$1.9 eV for the $^1(5\sigma\rightarrow\pi^*_{CL})$ transition. This is slightly larger than the values reported elsewhere.[26,27] However, we have also shown that this excitation energy is sensitive to the Pt–C bond length. Indeed, in the work of Freund *et al.*[26] shorter Pt–C bond lengths were used, leading to a decrease in the excitation energy. Our analysis indicates that this transition is of $^1(5\sigma\rightarrow\pi^*_{CL})$ character, and the $^1(5\sigma\rightarrow\pi^*_{CO})$ excitation is blueshifted by a greater amount. The magnitude of this blueshift reflects the degree to which the 5σ orbital is lowered on

adsorption. The work of Klüner *et al.*[29,30] reported the $^1(5\sigma \rightarrow \pi^*)$ excitation to lie at 9.8 eV in the threefold site, which is close to their computed gas-phase value. With a small cluster model, our calculations predict a $^1(5\sigma \rightarrow \pi^*_{\mathrm{CL}})$ excitation which is close to the gas-phase value. Although, a blueshift is observed using larger models of the surface. Again, the present, calculations also predict the $^1(5\sigma \rightarrow \pi^*_{\mathrm{CO}})$ excitation to lie higher in energy. Smaller shifts are observed for excitations from the 1π, and the $^1(4\sigma \rightarrow \pi^*)$ excitations lie above 12.5 eV.

The shifts in excitation energies relative to gas phase can, to a large extent, be interpreted based on the changes in $4\sigma, 1\pi$, and 5σ orbital energies (Fig. 2). The greatest blueshift in the $^1(5\sigma \rightarrow \pi^*_{\mathrm{CO}})$ transition is predicted for the on-top binding site. In this binding site there is the greatest lowering of the 5σ orbital energy. Changes in orbital energies can also be used to rationalize the variation in excitation energies due to binding geometry. In this work, larger cluster models of the surface have been studied than previously possible. Although convergence of the excitation energies with respect to the size of the cluster model has not be reached, they do begin to stabilize. This suggests that converged values may be attained with cluster models not too much larger than the ones used here. The sensitivity of the computed excitation energies to the geometry of the adsorbed CO means that very precise structures are required for high accuracy.

From the simulation of the electronic spectrum, assignment of the bands observed in EELS can be made. The band at low energy (5–7 eV) arises from $^1(d \rightarrow R)$ and $^1(d \rightarrow \pi^*)$ excitations. This band can wash out the band at 8.5 eV. Where the band at 8.5 eV is observed, our calculations indicate that it is also due to excitations from the metal *d* band and not a $^1(5\sigma \rightarrow \pi^*)$ excitation. This transition is less intense and appears at higher energy. This is particularly true for the on-top and bridge binding sites, which CO occupies preferentially on Pt(111). The high energy bands have contributions from many transitions, including $^1(5\sigma \rightarrow \pi^*)$, $^1(1\pi \rightarrow \pi^*)$, $^1(4\sigma \rightarrow \pi^*)$, and Rydberg excitations. This is probably the reason for the many different proposed assignments of these bands.

ACKNOWLEDGMENTS

This work was supported by the Engineering and Physical Sciences Research Council through the award of an Advanced Research Fellowship (Grant No. GR/R77636) and a Joint Research Equipment Initiative grant (Grant No. GR/R62052).

[1]Y.-T. Wong and R. Hoffmann, J. Phys. Chem. **95**, 859 (1991).
[2]G. M. Goncher and C. B. Harr, J. Chem. Phys. **77**, 3767 (1982).
[3]C. J. Chen and R. M. Osgood, Appl. Phys. A: Solids Surf. **31**, 171 (1983).
[4]G. Ritchie and E. Burstein, Phys. Rev. B **24**, 4843 (1981).
[5]G. Blyholder, J. Phys. Chem. **68**, 2772 (1964).
[6]J. Koutecky and P. Fantucci, Chem. Rev. (Washington, D.C.) **86**, 539 (1986).
[7]J. Li, B. Schiott, R. Hoffmann, and D. M. Proserpio, J. Phys. Chem. **94**, 1554 (1990).
[8]P. Hu, D. A. King, M.-H. Lee, and M. C. Payne, Chem. Phys. Lett. **246**, 73 (1995).
[9]B. Hammer, Y. Morikawa, and J. K. Nøskov, Phys. Rev. Lett. **76**, 2141 (1996).
[10]P. H. T. Philipsen, E. van Lenthe, J. G. Snijders, and E. J. Baerends, Phys. Rev. B **56**, 13556 (1997).
[11]H. Aizawa and S. Tsuneyuki, Surf. Sci. **399**, L364 (1998).
[12]R. A. Olsen, P. H. T. Philipsen, and E. J. Baerends, J. Chem. Phys. **119**, 4522 (2003).
[13]S.-S. Sung and R. Hoffmann, J. Am. Chem. Soc. **107**, 578 (1985).
[14]S. Ishii, Y. Ohno, and B. Viswanathan, Surf. Sci. **161**, 349 (1985).
[15]S. Ohnishi and N. Watari, Phys. Rev. B **49**, 14619 (1994).
[16]A. Fölisch, M. Nyberg, P. Bennich, L. Tiguero, J. Hasselström, O. Karis, L. G. M. Pettersson, and A. Nilsson, J. Chem. Phys. **112**, 1946 (2000).
[17]F. P. Netzer, J. U. Mack, E. Bertel, and J. A. D. Matthew, Surf. Sci. **160**, L509 (1985).
[18]P. Avouris and J. E. Demuth, Annu. Rev. Phys. Chem. **34**, 49 (1984).
[19]P. Avouris and J. E. Demuth, Surf. Sci. **158**, 21 (1985).
[20]P. Avouris, N. J. Dinard, and J. E. Demuth, J. Chem. Phys. **80**, 191 (1984).
[21]T. Fauster and F. J. Himpsel, Phys. Rev. B **27**, 1390 (1983).
[22]J. Rogozik, H. Scheidt, V. Dose, K. C. Prince, and A. M. Bradshaw, Surf. Sci. **145**, L481 (1984).
[23]K. Akimoto, Y. Sakisaka, M. Nishijima, and M. Onchi, Surf. Sci. **88**, 109 (1979).
[24]F. P. Netzer and J. A. D. Matthew, Surf. Sci. **81**, L651 (1979).
[25]G. W. Rubloff and J. L. Freeouf, Phys. Rev. B **17**, 4680 (1978).
[26]H.-J. Freund, R. P. Messmer, W. Spiess, H. Behner, G. Wedler, and C. M. Kao, Phys. Rev. B **33**, 5228 (1986).
[27]Y. Mochizuki, K. Tanaka, K. Ohno, and H. Tatewaki, Phys. Rev. B **39**, 11907 (1989).
[28]H. Nakatsuji, H. Morita, H. Nakai, Y. Murata, and K. Fukutani, J. Chem. Phys. **104**, 714 (1996).
[29]T. Klüner, N. Govind, Y. A. Yang, and E. A. Carter, Phys. Rev. Lett. **86**, 5954 (2001).
[30]T. Klüner, N. Govind, Y. A. Yang, and E. A. Carter, J. Chem. Phys. **116**, 42 (2002).
[31]S. Corni and J. Tomasi, J. Chem. Phys. **117**, 7266 (2002).
[32]N. A. Besley, Chem. Phys. Lett. **390**, 124 (2004).
[33]P. J. Hay and W. R. Wadt, J. Chem. Phys. **82**, 299 (1985).
[34]P. J. Stephens, F. J. Devlin, C. F. Chabalowski, and M. J. Frisch, J. Phys. Chem. **98**, 11623 (1994).
[35]P. S. Bagus and W. Muller, Chem. Phys. Lett. **115**, 540 (1985).
[36]S. Hirata and M. Head-Gordon, Chem. Phys. Lett. **314**, 291 (1999).
[37]R. E. Stratmann, G. E. Scuseria, and M. J. Frisch, J. Chem. Phys. **109**, 8218 (1998).
[38]P. J. Feibelman, B. Hammer, J. K. Nøskov, F. Wagner, M. Scheffler, R. Stumpf, R. Watwe, and J. Dumesic, J. Phys. Chem. B **105**, 4018 (2001).
[39]D. Geschke, T. Bastug, S. Fritzsche, W.-D. Sepp, B. Fricke, S. Varga, and J. Anton, Phys. Rev. B **64**, 235411 (2001).
[40]W. J. Hehre, R. Ditchfield, and J. A. Pople, J. Chem. Phys. **56**, 2257 (1972).
[41]T. H. Dunning, Jr., J. Chem. Phys. **90**, 1007 (1989).
[42]R. A. Kendall, T. H. Dunning, Jr., and R. J. Harrison, J. Chem. Phys. **96**, 6796 (1992).
[43]P. J. Hay and W. R. Wadt, J. Chem. Phys. **82**, 270 (1985).
[44]J. Kong, C. A. White, A. I. Krylov *et al.*, J. Comput. Chem. **21**, 1532 (2000).
[45]D. J. Tozer and N. C. Handy, J. Chem. Phys. **109**, 10180 (1998).
[46]A. D. Dreuw, J. L. Weisman, and M. Head-Gordon, J. Chem. Phys. **119**, 2943 (2003).
[47]J. Rogozik and V. Dose, Surf. Sci. **176**, L847 (1986).
[48]P. D. Johnson, D. A. Wesner, J. W. Davenport, and N. V. Smith, Phys. Rev. B **30**, 4860 (1984).
[49]T. Hertel, E. Knoesel, E. Hasselbrink, M. Wolf, and G. Ertl, Surf. Sci. **317**, L1147 (1994).
[50]S. Ivanov, S. Hirata, and R. J. Bartlett, Phys. Rev. Lett. **83**, 5455 (1999).
[51]E. S. Nielson, P. J. Jørgensen, and J. Oddershede, J. Chem. Phys. **23**, 6238 (1980).